Development of Dilated Cardiomyopathy and Impaired Calcium Homeostasis with Cardiac-Specific Deletion of ESRRβ

Glenn C. Rowe[1,5,#], Angeliki Asimaki[2], Evan L. Graham[1,6], Kimberly D. Martin[3], Kenneth Margulies[4], Saumya Das[1,6], Jeffery Saffitz[2], and Zoltan Arany[1,8,#]

[1]Cardiovascular Institute, Department of Medicine, Beth Israel Deaconess Medical Center, and Harvard Medical School, Boston MA 02215, USA.
[2]Pathology, Beth Israel Deaconess Medical Center, and Harvard Medical School, Boston MA 02215, USA.
[3]Department of Epidemiology, University of Alabama at Birmingham, Birmingham AL 35294.
[4]Perelman School of Medicine, University of Pennsylvania, Philadelphia PA 19104

Current Address
[5]Division of Cardiovascular Diseases, Department of Medicine, University of Alabama at Birmingham, Birmingham, AL 35294
[6]Department of Cell and Molecular Biology, Karolinska Institutet, Von Eulers Väg 3, 117177 Stockholm, Sweden
[7]Division of Cardiology, Department of Medicine, Massachusetts General Hospital, and Harvard Medical School, Boston MA 02215, USA
[8]Perelman School of Medicine, University of Pennsylvania, Philadelphia PA 19104

[#] - Addresses for correspondence
Glenn C. Rowe, PhD
Division of Cardiovascular Diseases,
Department of Medicine,
University of Alabama at Birmingham,
1918 University Blvd, MCLM 285,
Birmingham, AL 35294
USA
Tel # 205-975-0100
Email gcrowe@uab.edu

Zoltan Arany, MD PhD
Perelman School of Medicine,
University of Pennsylvania,
3400 Civic Blvd, Philadelphia PA 19104
USA
Tel# 215-898-3482
Email zarany@mail.med.upenn.edu

Running Title: Cardiac-Specific Deletion of ESRRβ Develop DCM

52 **Keywords**: estrogen-related receptor; dilated cardiomyopathy; calcium handling

Abstract

Mechanisms underlying the development of Idiopathic Dilated Cardiomyopathy (DCM) remain poorly understood. Using transcription factor expression profiling, we identified estrogen-related receptor beta (ESRRβ), a member of the nuclear receptor family of transcription factors, as highly expressed in murine hearts and other highly oxidative striated muscle beds. Mice bearing cardiac-specific deletion of ESRRβ (MHC-ERRB KO) develop dilated cardiomyopathy and sudden death at approximately 10 months of age. Isolated adult cardiomyocytes from the MHC-ERRB KO mice showed an increase in calcium sensitivity and impaired cardiomyocyte contractility, which preceded echocardiographic cardiac remodeling and dysfunction by several months. Histological analyses of myocardial biopsies from patients with various cardiomyopathies revealed that ESRRβ protein is absent from the nucleus of cardiomyocytes from patients with DCM, but not other forms of cardiomyopathy (ischemic, hypertrophic and arrhythmogenic right ventricular cardiomyopathy). Taken together these observations suggest that ESRRβ is a critical component in the onset of dilated cardiomyopathy by affecting contractility and calcium balance.

New and Noteworthy

ESRRβ is highly expressed in the heart and cardiac specific deletion results in the development of a dilated cardiomyopathy (DCM). ESRRβ is mislocalized in human myocardium samples with DCM, suggesting a possible role for ESRRβ in the pathogenesis of DCM in humans.

Introduction

Heart failure is a major health concern and a leading cause of death in the developing world. Idiopathic dilated cardiomyopathy (DCM) occurs in the absence of epicardial or other known cardiac diseases. Its etiology is often genetic, most frequently involving mutations in *TTN*, the gene encoding for the large sarcomeric protein titin(19, 20). However, the molecular triggers that lead to the development of DCM, often later in adult life, remain poorly understood. The heart is a highly metabolic organ, one third of which is composed of mitochondria, and consuming up to 20% of systemic oxygen consumption at rest. Mutations in various components of mitochondrial function lead to dilated cardiomyopathy(21, 36), underscoring the importance of oxidative metabolism in the heart. Some pathways that negatively affect metabolism have also been suggested as being contributors to the development of more common forms of cardiomyopathy (21, 32), and human late-stage heart failure reveals defects in oxidative metabolism(11, 24), and is often considered to be “energy-starved” (22, 31, 33).

In order to identify novel transcriptional regulators of cardiac and oxidative metabolism, we performed a gene expression screen in various oxidative striated muscles beds and cells. To accomplish this, we took advantage of the PGC-1α transcriptional coactivator as a potent regulator of oxidative metabolism. PGC-1α was first identified in a yeast two-hybrid screen looking for factors that interact with the PPARγ transcription factor in brown adipocyte cells(37), and has since emerged as a critical regulator of oxidative metabolism and mitochondrial function (27, 40, 44). Ectopic overexpression of PGC-1α in cardiomyocytes in both cell culture and *in vivo* markedly increases oxygen consumption capacity and fatty acid oxidation with a concomitant decrease in glucose oxidation(25, 47). Conversely PGC-1α null mice exhibit impaired bioenergetics in cardiomyocytes, associated with decreased ATP generation(3, 26). Moreover, under conditions of stress such as aortic constriction, PGC-1α null hearts are

more susceptible to heart failure(4). PGC-1α does not bind to DNA directly, and requires the induction and subsequent activation of transcription factors to mediate its effect on gene transcription.

Here we identify estrogen-related receptor beta (ESRRβ) as being highly expressed in conditions of high oxidative metabolic capacity. We show that mice lacking cardiac ESRRβ develop DCM in mid-life, preceded by pronounced defects in calcium handling and cellular contractility. Lastly, we show that ESRRβ nuclear expression is lost in human DCM suggesting a role in the pathogenesis of human DCM.

Methods and Materials

Human studies. All procedures were approved by the University of Pennsylvania and Beth Israel Deaconess Medical Center Institutional Review Boards (IRB).

Animal studies. All animal experiments were performed according to procedures approved by the Beth Israel Deaconess Medical Center's Institutional Animal Care and Use Committee. Mice floxed for exon 2 of ESRRβ ($ESRRB^{flox/flox}$) as previously described(9),and mice expressing Cre recombinase under the control of the alpha-myosin heavy chain promoter (α-MHC-$Cre^{+/-}$) as previously described (1, 4, 35), were obtained from (Jackson Labs Stock # 007674 and 018972 respectively) were crossed to generate a cardiac-specific ESRRβ KO (MHC-ERRB KO) ($ESRRB^{flox/flox}$/α-MHC-$Cre^{+/-}$) animals. Muscle-specific PGC-1α transgenic mice were previously described(29). All animals were maintained on C57BL/6 background. Mice were maintained on standard rodent chow with a 12-h light and dark cycles. Echocardiogrpahy were performed on non-anesthetized mice using a Vivid FiVe ECHO system (GE Medical Systems), M-mode recordings at the mid-ventricle region of the heart were taken. Unless otherwise stated animals were taken at 4 months, 6 months and 9 months.

Gene expression studies. Total RNA was isolated from tissues and cells using Trizol

(Invitorgen) following manufacturer's instructions and subjected to reverse transcription using High Capacity Reverse Transcription (Invitrogen). Quantitative real-time PCR was performed on cDNA using the intercalating fluorescent dye SYBR green (BioRad) with gene specific primers using a CFX 384 Touch real-time PCR machine (BioRad). Relative expression was determined using the Comparative cycle threshold method ($2^{-\Delta\Delta Ct}$) with 36B4, HPRT and TBP used as housekeeping genes. For human samples used for gene expression studies, whole human hearts were procured from two separate patient groups: patients with end-stage heart failure who received heart transplants and hearts from brain dead organ donors. The failing hearts (dilated CM n=13 and ischemic CM n=13) came from patients undergoing transplants at the University of Pennsylvania. Hearts from brain-dead organ donors were made available through the Gift of Life Donor Program (Philadelphia, PA) and the selected cases had no history of heart failure or evidence of significant myocardial pathology (non-failing controls n=13). Tissue from age-matched individuals with no pathological or clinical evidence of heart disease were subjected to the same protocol and used as controls.

Complex IV and Citrate synthase enzymatic activity. Heart samples were snap frozen with liquid nitrogen until ready to process. Complex IV activity was measured by oxidation of cytochrome c as previously described (6, 43). Citrate synthase activity was measured as previously described (42).

Cardiomyocyte calcium Imaging and contractility. Adult murine ventricular cardiomyocytes from wild type and transgenic mice were isolated as previously described(16) and loaded with 0.25μg Fura2-AM for subsequent calcium transient analysis using the MMSYS IonOptix imaging system. Isolated cardiomyocytes were stimulated with 15V at a frequency of 5Hz to induce uniform cell contraction at 37 °C. Contractility measurements were calculated using sarcomere shortening distances from real-time phase-contrast images. Intracellular calcium concentrations were calculated

from the ratio of bound to unbound Fura2-AM. These measurements were used to determine contractile and calcium transients depicting the cell's overall contractility or the flux of calcium across the cell membrane. Both contractility measurements and calcium transients were recorded for 5-10 minutes, at which point each curve was averaged to generate a representative contractile or calcium transient plot for each cell recorded. These plots were then analyzed using a monotransient data analysis algorithm to generate surrogate parameters for systolic and diastolic function for that cell.

Immunofluorescence staining of human heart samples. De-identified samples came from native hearts of patients who had undergone cardiac transplantation due to end-stage heart failure. Transmural sections of right and left ventricles from patients with hypertrophic (n=3), with dilated (n=4) and with ischemic (n=3) cardiomyopathies were analyzed. The second set of samples came from patients who had died suddenly and diagnosed with arrhythmogenic right ventricular (n=3) cardiomyopathy at postmortem examination. Tissue from age-matched individuals with no pathological or clinical evidence of heart disease were subjected to the same protocol and used as controls (n=3). Samples were processed in formalin and subjected to paraffin embedding. In preparation for immunofluorescence microscopy, deparaffinized, rehydrated slide-mounted sections were heated in citrate buffer (10mmol/l, pH 6.0) to enhance specific immunostaining. After being cooled to room temperature, the tissue sections were simultaneously permeabilized and blocked by incubating them in phosphate-buffered saline (PBS) containing 1% Triton X-100, 3% normal goat serum and 1% bovine serum albumin. The sections were then incubated first with a primary antibody and then with indocarbocyanine-conjugated goat anti-rabbit IgG. Primary antibodies included polyclonal rabbit anti-ERR1 (Thermo Fisher), polyclonal rabbit anti-ERRB (Thermo Fisher) and polyclonal rabbit N-Cadherin (Sigma). Immunostained

preparations were analyzed by confocal microscopy (Sarastro Model 2000, Molecular Dynamics) as previously described(41).

Statistical analysis. The data are presented as means ± standard error of the mean (SEM). Statistical analysis was performed with Student's t test for *in vitro* experiments and ANOVAs for all *in vivo* experiments. Univariate statistics were performed on Contraction and calcium variables to assess distribution of values. For each time point, the effect of ERRB KO status on each response variable was modeled using generalized estimating equations, accounting for the distribution of each response variable as well as nesting of cell samples within the same mouse. For comparisons of presence or absence of nuclear ESRRB on human biopsies, the nonparametric Chi-Square test of association was used. *P* values of less than 0.05 were considered statistically significant.

Results

Identification of ESRRβ in a screen for transcription factors highly expressed in oxidative muscle.

We sought to identify transcription factors that were differentially expressed in striated muscle beds of high versus low oxidative capacity. We utilized a high throughput screen in which the expression of ~2000 known or putative transcription factors are screened by qPCR(17, 18, 38). We compared the expression of the TFs in murine muscle or cells in 4 contexts: 1.) slow twitch soleus muscle versus fast twitch quadriceps muscle, 2.) quadriceps vs cardiac muscle, 3.) PGC-1α overexpression in cultured myotubes versus GFP-only expression, and 4.) transgenic PGC-1α overexpression in quadriceps versus littermate control. As shown in Figure 1A, five TFs were found in all four cases to be more highly expressed in the more oxidative tissue or cells. The five TFs included PGC-1α itself, as well as PPARα, a nuclear receptor well-known to control programs of fatty

acid oxidation in these contexts (8, 28). The most highly differentially expressed TF after PGC-1α was ESRRβ (Figure 1B). ESRRβ is a member of the three-member ESRR family of transcription factors, named for their primary homology to the estrogen receptor (ESR), though importantly estrogen likely does not bind to members of the ESRR family. ESRRα and ESRRγ have been studied extensively as drivers of oxidative metabolism in muscle and other tissues (15, 46), but little is known of the role of ESRRβ in muscle tissues. qPCR analysis of RNA isolated from various tissues revealed that ESRRβ is most highly expressed in the heart, followed by muscle, kidney, testes, brain, and stomach, all of which are highly oxidative tissues (Figure 1C).

Cardiac-Specific Deletion of ESRRβ leads to profound adult-onset dilated cardiomyopathy.

ESRRβ is most highly expressed in the heart, yet its role in cardiac physiology is unknown. To determine the role of ESRRβ in the heart we generated a cardiac-specific knockout of ESRRβ using the alpha-myosin heavy chain (α-MHC) promoter driving the expression of Cre recombinase and ESRRβ floxed mice to obtain MHC-ERRB KO animals. The MHC-ERRB KO animals had a 95% reduction in ESRRβ in the heart, with no loss of ESRRβ expression in skeletal muscle and kidney (Figure 1D). The significant deletion of ESRRβ with the α-MHC promoter suggests that in the heart ESRRβ is primarily expressed within cardiomyocytes and not other cells. The MHC-ERRB KO mice were born at Mendelian ratios with no overt phenotype at birth. However, the MHC-ERR β KO had poor survival rates after 9 to 10 months of age as quantified by Kaplan-Meier survival curve analysis (Figure 2A). Gross analysis of the hearts from these animals at 9 months revealed a significantly enlarged heart (Figure 2B). Gravimetric analysis of heart parameters revealed a significant increase in heart weight to body

weight (Figure 2C) as well as heart weight to tibial length (Figure 2D). qPCR analysis of ventricular RNA revealed an increase in the expression of ANF, BNP and β-MHC, and a trend towards a decrease in α-MHC (Figure 2E). These data indicate a heart failure gene signature in the hearts of the MHC-ERRB KO. Masson's Trichrome staining of the left ventricle revealed a significant increase in fibrosis (Figure 2F). This increase in fibrosis was confirmed by qPCR analysis revealing a significant increase in collagen and other fibrotic markers (Figure 2G).

We next sought to evaluate cardiac function in the MHC-ERRB KO by non-invasive echocardiography (ECHO). Two dimensional M-mode analysis of the ECHOs revealed a significant dilated cardiomyopathy (Figure 3A) associated with a decrease in anterior wall thickness (AW) (Figure 3B), significantly increased left ventricular end systolic diameter (LVESD) (Figure 3C) and left ventricular end diastolic diameter (LVEDD) (Figure 3D), and a 60% decrease in fractional shortening (FS) (Figure 3E). This decrease in cardiac function is associated with a decrease in OXPHOS genes and FAO genes as revealed by qPCR analysis (Figure 3F and 3G), and a small but not statistically significant decline in complex IV activity and citrate synthase activity (Figure 3H and 3I). Interestingly, no evidence of cardiac dysfunction on echocardiography was seen at earlier time points in life, including 4 and 6 months (Figure 4A-H). We did not observe any changes in expression of the other ESRR family members (Figure 4I) or genes involved in OXPHOS (Figure 4J), although at 6 months the expression of ANF and BNP did start to increase (Figure 4K). Taken together these data demonstrate that loss of ESRRβ result in the development of pronounced dilated cardiomyopathy during mid-to-late murine life.

Cardiomyocytes from MHC-ERRB KO mice exhibit impaired contractility and calcium handling.

We next sought to determine whether the loss of ESRRβ had a cell autonomous effect on cardiomyocyte function. Ventricular cardiomyocytes were isolated from MHC ERRB KO mice at 4, 6 and 9 months of age and compared to wild type, age-matched littermates (Figure 5A-C). Length measurements of the isolated cardiomyocytes revealed a significant increase in sarcomere length only after 9 months (Figure 5C), consistent with the timing of echocardiographic phenotype of left ventricular dilation (Figure 3). However, this structural defect was preceded at 6 months by contractile dysfunction evidenced by a decrease in both contractile distance (sarcomere shortening, Figure 5D-F) and speed of contraction (Figure 5G-I), both of which persisted at the 9-month time point. Evidence of cell-autonomous contractile defects is thus apparent in MHC-ERRB KO mice as early as 6 months (Figure 5E and 5H).

To evaluate calcium handling in these same cardiomyocytes, we measured calcium release and uptake using Fura2AM fluorescent probes (Figure 6A-F). We found that dysfunction in calcium handling began as early as 4 months, with Ca^{2+} release being significantly decreased (Figure 6A), with a coincident trend in decrease in Ca^{2+} uptake (Figure 6D). Curiously, the observed decreases in calcium release and uptake at 4 months (Figure 6A, D) is reversed and becomes a markedly increased calcium release and uptake at 6 months of age (Figure 6B,E), which persists at 9 months of age (Figure 6C,F). This increase in calcium release was associated with a time dependent increase in calcium transients at 6 and 9 months (Figure 6G-I). Taken together, these data indicate that deregulation of the excitation-contraction coupling apparatus appear in MHC-ERRB KO mice as early as four months of age, significantly preceding both cellular contractile defects and echocardiographic abnormalities.

ESRRβ Protein Localization in Human Heart Failure Sections.

We next sought to determine if ESRRβ localization was affected in human heart failure. Samples were obtained from native hearts at the time of transplant from patients with diagnoses of ischemic cardiomyopathy (iCM), hypertrophic cardiomyopathy (HCM), idiopathic dilated cardiomyopathy (DCM) or postmortem samples of patients who died suddenly with a diagnosis of arrhythmogenic right ventricular cardiomyopathy (ARVC), and compared to control donor hearts. Transmural sections immunostained for ESRRβ revealed the presence of ESRRβ in the nucleus in all sections with the exception of the DCM samples (Figure 7A). The pattern of absent ESRRβ staining was seen in 4 of 4 DCM samples, but in zero of 3 control and other cardiomyopathy samples ($P<0.01$). Moreover, this localization of ESRRβ was specific, as neither ESRRα (nuclear) (Figure 7B) nor N-cadherin (membrane-bound) revealed any differences in protein distribution (Figure 7C). Interestingly, in contrast to ESRRα, we did not observe any significant difference in expression of ESRRβ mRNA in cardiac samples from patients with DCM or iCM, compared to donor hearts (Figure 7D), indicating that ESRRβ protein expression, stability, or localization is affected post-transcriptionally. Taken together the data indicate that ESRRβ protein is undetectable or mislocalized in human DCM.

Discussion

The PGC-1s and many of their downstream transcriptional regulators have been shown to be important in maintaining cardiac metabolic function (5, 39, 40). Members of the estrogen-related receptor (ESRR) family of orphan receptors have emerged as being important regulators of cardiac function(46). While bearing significantly homology to the estrogen receptor, estrogen-related receptors do not bind estrogen and consist of three members α, β, and γ(15). ESRRα has been studied extensively in the heart and other metabolic tissues(15), and has been shown to be a key component of the gene regulatory machinery that regulates mitochondrial biogenesis and function in these

tissue. ESRRγ has been studied much less extensively, but most data indicate a significant overlap in function between ESRRα and ESRRγ(12). Moreover, germline deletion of ESRRγ results in post-natal lethality presumably due to impaired cardiac function(2). ESRRβ appears to have very different role compared to the other family members, despite their homology. Germline deletion of ESRRβ is embryonic lethal due to abnormal placental formation during early embryogenesis(30). However, the role of ESRRβ in cardiac function was unknown.

Here we identify ESRRβ as a key regulator in the development of the dilated cardiomyopathy. The precise mechanism by which loss of ESRRβ leads to CM remains uncertain. Our data indicate that impaired calcium homeostasis precedes evidence of defects in contractility both in cell culture and in intact animals, suggesting that ESRRβ may regulate calcium handling. The calcium handling phenotype suggested an early defect in Ca release and uptake, which may account for the alterations in contractility noted. The later changes that suggested an increase in Ca release and uptake may be secondary or adaptive, although the mechanisms are still to be elucidated. However, we did not find that expression of known calcium-handling genes, such as RYR, SERCA2 or PL, was altered in hearts lacking ESRRβ at the time that calcium-handling defects appear. It is possible that ESRRβ affects calcium homeostasis via mechanisms other than regulating gene expression. Such non-genomic mechanisms have been noted for various nuclear receptors, including estrogen receptor(7, 10, 34). ESRRβ is also well recognized as a pluripotency factor, able to substitute for classical Yamanaka factors in certain contexts (13, 14, 23). However, it seems unlikely that cardiomyopathy in the ESRRβ KO hearts stems from loss of pluripotency, because cardiomyocytes in adult hearts replicate very little.

Our results suggest that loss of ESRRβ may contribute to the development of DCM. Nuclear receptors, including ESRRβ, are unique transcription factors in that they

are typically ligand-activated. Nuclear receptors are therefore more easily drugged targets, providing a potentially amenable translational avenue. An endogenous ligand for ESRRβ is not known, but various synthetic ligands can activate it (45, 48). It will therefore be of great interest to test these ligands in models of DCM.

It is interesting that the absence of nuclear ESRRβ was noted in idiopathic DCM samples, but not in other causes of dilated cardiomyopathy, suggesting that: 1) dilation of the heart *per se* does not cause loss of nuclear ESRRβ, and 2) loss of nuclear ESRRβ may uniquely contribute to the pathogenesis of idiopathic DCM. As noted, at least a quarter of idiopathic DCM cases are caused by truncating mutations in *TTN*, the gene encoding the sarcomeric protein titin. How mutations in a sarcomeric protein should affect the nuclear localization of a transcription factor is unclear. Evaluation of ESRRβ location and function in mouse models bearing mutations in *ttn*, once available, will therefore be of interest. Therefore, targeting ESRRβ with specific agonist could provide a new powerful intervention in the treatment of dilated cardiomyopathy.

Acknowledgements

Author contributions: G.C.R. and Z.A. designed research; G.C.R., A.A., E.L.G., and K.M. performed research; G.C.R., A.A., E.L.G., K.M., K.D.M., S.D., and Z.A. analyzed data, K.M. and J.S. provided samples, G.C.R. and Z.A. wrote the paper. This work was supported by grants from the NIH, NIAMS to G.C.R. (AR062128) and NHLBI to Z.A (HL094499, HL126797) and the American Heart Association to Z.A. We are grateful to the UAB DRC BARB Core, supported by NIH NIDDK (DK079626), for help with electron transport complex activity assays.

Figure Legends

Figure 1. Identification of ESRRβ in Cardiac metabolism. A.) Schematic of high-throughput qPCR screen. B.) Fold expression of upregulated genes in skeletal muscle of MCK-PGC-1Tg compared to control littermates. C.) Relative ESRRβ mRNA expression in various tissues. D.) Relative ESRRβ mRNA expression in Heart, Skeletal Muscle and Kidney of MHC-ERRBKO and Control mice at 2 months. Data are presented as mean ± SEM; n = 4-6 per group; * - $P < 0.05$ compared to control animals.

Figure 2. Cardiac Phenotype of MHC-ERRB KO mice. A.) Kaplan-Meier survival curve of MHC-ERRBKO animals. B.) Gross heart anatomy of the MHC-ERRBKO animals compared to control animals. C.) Heart weight normalized to body weight (HW/BW). D.) Heart weight normalized to tibial length (HW/TL). E.) mRNA expression of heart failure markers. F.) Masson Trichrome staining. G.) qPCR expression of markers of fibrosis of MHC-ERRBKO and control animals at 9 to 10 months of age. Data are presented as mean ± SEM; n = 4-6 per group; * - $P < 0.05$ compared to control animals.

Figure 3. Non-invasive ECHOs of MHC-ERRBKO. A.) Sample M-mode echocardiograms from the left ventricle (LV). B.) Anterior wall thickness (AW). C.) Left ventricular end systolic diameter (LVESD). D.) Left ventricular end diastolic diameter (LVEDD). E.) Percent fractional shortening (%FS). F.) qPCR expression of OXPHOS genes. G.) qPCR expression of FAO genes. H.) Complex IV enzymatic activity. I.) Citrate synthase activity of MHC-ERRBKO and control animals. Data are presented as mean ± SEM; n = 4-6 per group; * - $P < 0.05$ compared to control animals.

Figure 4. Normal Function in Younger MHC-ERRBKO Animal. A.) Sample M-mode echocardiograms from the left ventricle (LV) B.) Left ventricular end systolic diameter (LVESD). C.) Left ventricular end diastolic diameter (LVEDD). D.) Percent fractional shortening (%FS) at 4 months. E.) Sample M-mode echocardiograms from the left ventricle (LV), F.) Left ventricular end systolic diameter (LVESD), G.) Left ventricular end diastolic diameter (LVEDD). H.) Percent fractional shortening (%FS) at 6 months. I.)

qPCR expression of ESRR isoforms. J.) qPCR expression of OXPHOS genes. K.) mRNA expression of heart failure markers. Data are presented as mean ± SEM; n = 4-6 per group; * - $P < 0.05$ compared to control animals.

Figure 5. Decreased contractility in ERRB deleted cardiomyocytes. A-C.) Sarcomere length (micrometers). D-F.) Maximum contraction length/distance (micrometers). G-I.) Contraction speed (micrometers/second) of MHC-ERRBKO and control mice at 4, 6 and 9 months. Data are presented as whisker plots with medians and min/max values; (N = 3 – 4 animals per group; n = 12 – 20 cells per animals); * - $P < 0.05$ and ** - $P < 0.001$ compared to control animals.

Figure 6. Impaired cardiomyocytes calcium homeostasis with ESRRβ deletion. A-C.) Calcium release (Fura2/sec). D-F.) Calcium uptake (Fura2/sec). G-I) Calcium transients traces (340/380nm) of MHC-ERRBKO and control mice at 4, 6 and 9 months. Data are presented as whisker plots with medians and min/max values; (N = 3 – 4 animals per group; n = 12 – 20 cells per animals); * - $P < 0.05$ and ** - $P < 0.001$ compared to control animals.

Figure 7. ESRRβ localization and expression in human heart samples. A.) Immunostaining for ESRRβ , B.) ESRRα, and C.) N-Cadherin in human transmural sections from arrhythmogenic right ventricular cardiomyopathy (ARVC) (n=3), ischemic cardiomyopathy (iCM) (n=3), hypertrophic cardiomyopathy (HCM) (n=3), dilated cardiomyopathy (DCM) (n=4) and control donor (n=3) staining of human hearts. D.) mRNA expression of ESRR isoforms and PGC-1 in non-failing, ischemic cardiomyopathy (iCM) (n=13) and dilated cardiomyopathy (DCM) (n=13). * - $P < 0.05$

References

1. **Agah R, Frenkel PA, French BA, Michael LH, Overbeek PA, and Schneider MD**. Gene recombination in postmitotic cells. Targeted expression of Cre recombinase provokes cardiac-restricted, site-specific rearrangement in adult ventricular muscle in vivo. *J Clin Invest* 100: 169-179, 1997.

2. **Alaynick WA, Kondo RP, Xie W, He W, Dufour CR, Downes M, Jonker JW, Giles W, Naviaux RK, Giguere V, and Evans RM**. ERRgamma directs and maintains the transition to oxidative metabolism in the postnatal heart. *Cell Metab* 6: 13-24, 2007.
3. **Arany Z, He H, Lin J, Hoyer K, Handschin C, Toka O, Ahmad F, Matsui T, Chin S, Wu P, Rybkin I, Shelton J, Manieri M, Cinti S, Schoen F, Bassel-Duby R, Rosenzweig A, Ingwall J, and Spiegelman BM**. Transcriptional coactivator PGC-1 alpha controls the energy state and contractile function of cardiac muscle. *Cell metabolism* 1: 259-271, 2005.
4. **Arany Z, Novikov M, Chin S, Ma Y, Rosenzweig A, and Spiegelman BM**. Transverse aortic constriction leads to accelerated heart failure in mice lacking PPAR-gamma coactivator 1alpha. *Proc Natl Acad Sci U S A* 103: 10086-10091, 2006.
5. **Aubert G, Vega RB, and Kelly DP**. Perturbations in the gene regulatory pathways controlling mitochondrial energy production in the failing heart. *Biochim Biophys Acta* 1833: 840-847, 2013.
6. **Ballmann C, Tang Y, Bush Z, and Rowe GC**. Adult expression of PGC-1alpha and -1beta in skeletal muscle is not required for endurance exercise-induced enhancement of exercise capacity. *American journal of physiology Endocrinology and metabolism* 311: E928-E938, 2016.
7. **Bjornstrom L, and Sjoberg M**. Mechanisms of estrogen receptor signaling: convergence of genomic and nongenomic actions on target genes. *Mol Endocrinol* 19: 833-842, 2005.
8. **Burkart EM, Sambandam N, Han X, Gross RW, Courtois M, Gierasch CM, Shoghi K, Welch MJ, and Kelly DP**. Nuclear receptors PPARbeta/delta and PPARalpha direct distinct metabolic regulatory programs in the mouse heart. *J Clin Invest* 117: 3930-3939, 2007.
9. **Chen J, and Nathans J**. Estrogen-related receptor beta/NR3B2 controls epithelial cell fate and endolymph production by the stria vascularis. *Dev Cell* 13: 325-337, 2007.
10. **Cheskis BJ, Greger JG, Nagpal S, and Freedman LP**. Signaling by estrogens. *J Cell Physiol* 213: 610-617, 2007.
11. **Doenst T, Nguyen TD, and Abel ED**. Cardiac Metabolism in Heart Failure: Implications Beyond ATP Production. *Circ Res* 113: 709-724, 2013.
12. **Dufour CR, Wilson BJ, Huss JM, Kelly DP, Alaynick WA, Downes M, Evans RM, Blanchette M, and Giguere V**. Genome-wide orchestration of cardiac functions by the orphan nuclear receptors ERRalpha and gamma. *Cell Metab* 5: 345-356, 2007.
13. **Feng B, Jiang J, Kraus P, Ng JH, Heng JC, Chan YS, Yaw LP, Zhang W, Loh YH, Han J, Vega VB, Cacheux-Rataboul V, Lim B, Lufkin T, and Ng HH**. Reprogramming of fibroblasts into induced pluripotent stem cells with orphan nuclear receptor Esrrb. *Nature cell biology* 11: 197-203, 2009.
14. **Festuccia N, Osorno R, Halbritter F, Karwacki-Neisius V, Navarro P, Colby D, Wong F, Yates A, Tomlinson SR, and Chambers I**. Esrrb is a direct Nanog target gene that can substitute for Nanog function in pluripotent cells. *Cell Stem Cell* 11: 477-490, 2012.
15. **Giguere V**. Transcriptional Control of Energy Homeostasis by the Estrogen-Related Receptors. *Endocrine Reviews* 29: 677-696, 2008.
16. **Graham EL, Balla C, Franchino H, Melman Y, del Monte F, and Das S**. Isolation, culture, and functional characterization of adult mouse cardiomyoctyes. *J Vis Exp* e50289, 2013.
17. **Gray PA, Fu H, Luo P, Zhao Q, Yu J, Ferrari A, Tenzen T, Yuk DI, Tsung EF, Cai Z, Alberta JA, Cheng LP, Liu Y, Stenman JM, Valerius MT, Billings N, Kim HA, Greenberg ME, McMahon AP, Rowitch DH, Stiles CD, and Ma Q**. Mouse brain

organization revealed through direct genome-scale TF expression analysis. *Science* 306: 2255-2257, 2004.
18. **Gupta RK, Arany Z, Seale P, Mepani RJ, Ye L, Conroe HM, Roby YA, Kulaga H, Reed RR, and Spiegelman BM**. Transcriptional control of preadipocyte determination by Zfp423. *Nature* 464: 619-623, 2010.
19. **Herman DS, Lam L, Taylor MR, Wang L, Teekakirikul P, Christodoulou D, Conner L, DePalma SR, McDonough B, Sparks E, Teodorescu DL, Cirino AL, Banner NR, Pennell DJ, Graw S, Merlo M, Di Lenarda A, Sinagra G, Bos JM, Ackerman MJ, Mitchell RN, Murry CE, Lakdawala NK, Ho CY, Barton PJ, Cook SA, Mestroni L, Seidman JG, and Seidman CE**. Truncations of titin causing dilated cardiomyopathy. *N Engl J Med* 366: 619-628, 2012.
20. **Hinson JT, Chopra A, Nafissi N, Polacheck WJ, Benson CC, Swist S, Gorham J, Yang L, Schafer S, Sheng CC, Haghighi A, Homsy J, Hubner N, Church G, Cook SA, Linke WA, Chen CS, Seidman JG, and Seidman CE**. HEART DISEASE. Titin mutations in iPS cells define sarcomere insufficiency as a cause of dilated cardiomyopathy. *Science* 349: 982-986, 2015.
21. **Huss JM, and Kelly DP**. Mitochondrial energy metabolism in heart failure: a question of balance. *J Clin Invest* 115: 547-555, 2005.
22. **Ingwall JS**. On the control of metabolic remodeling in mitochondria of the failing heart. *Circ Heart Fail* 2: 275-277, 2009.
23. **Iseki H, Nakachi Y, Hishida T, Yamashita-Sugahara Y, Hirasaki M, Ueda A, Tanimoto Y, Iijima S, Sugiyama F, Yagami K, Takahashi S, Okuda A, and Okazaki Y**. Combined Overexpression of JARID2, PRDM14, ESRRB, and SALL4A Dramatically Improves Efficiency and Kinetics of Reprogramming to Induced Pluripotent Stem Cells. *Stem Cells* 34: 322-333, 2016.
24. **Karamanlidis G, Nascimben L, Couper GS, Shekar PS, del Monte F, and Tian R**. Defective DNA replication impairs mitochondrial biogenesis in human failing hearts. *Circ Res* 106: 1541-1548, 2010.
25. **Lehman JJ, Barger PM, Kovacs A, Saffitz JE, Medeiros DM, and Kelly DP**. Peroxisome proliferator-activated receptor gamma coactivator-1 promotes cardiac mitochondrial biogenesis. *J Clin Invest* 106: 847-856, 2000.
26. **Lehman JJ, Boudina S, Banke NH, Sambandam N, Han X, Young DM, Leone TC, Gross RW, Lewandowski ED, Abel ED, and Kelly DP**. The transcriptional coactivator PGC-1alpha is essential for maximal and efficient cardiac mitochondrial fatty acid oxidation and lipid homeostasis. *Am J Physiol Heart Circ Physiol* 295: H185-196, 2008.
27. **Leone TC, and Kelly DP**. Transcriptional control of cardiac fuel metabolism and mitochondrial function. *Cold Spring Harb Symp Quant Biol* 76: 175-182, 2011.
28. **Leone TC, Weinheimer C, and Kelly DP**. A critical role for the peroxisome proliferator-activated receptor alpha (PPARalpha) in the cellular fasting response: the PPARalpha-null mouse as a model of fatty acid oxidation disorders. *Proc Natl Acad Sci U S A* 96: 7473-7478, 1999.
29. **Lin J, Wu H, Tarr PT, Zhang CY, Wu Z, Boss O, Michael LF, Puigserver P, Isotani E, Olson EN, Lowell BB, Bassel-Duby R, and Spiegelman BM**. Transcriptional co-activator PGC-1 alpha drives the formation of slow-twitch muscle fibres. *Nature* 418: 797-801, 2002.
30. **Luo J, Sladek R, Bader JA, Matthyssen A, Rossant J, and Giguere V**. Placental abnormalities in mouse embryos lacking the orphan nuclear receptor ERR-beta. *Nature* 388: 778-782, 1997.
31. **Lygate CA, Schneider JE, and Neubauer S**. Investigating cardiac energetics in heart failure. *Exp Physiol* 98: 601-605, 2013.

32. **Neglia D, De Caterina A, Marraccini P, Natali A, Ciardetti M, Vecoli C, Gastaldelli A, Ciociaro D, Pellegrini P, Testa R, Menichetti L, L'Abbate A, Stanley WC, and Recchia FA**. Impaired myocardial metabolic reserve and substrate selection flexibility during stress in patients with idiopathic dilated cardiomyopathy. *Am J Physiol Heart Circ Physiol* 293: H3270-3278, 2007.
33. **Neubauer S**. The failing heart--an engine out of fuel. *N Engl J Med* 356: 1140-1151, 2007.
34. **Ordonez-Moran P, and Munoz A**. Nuclear receptors: genomic and non-genomic effects converge. *Cell Cycle* 8: 1675-1680, 2009.
35. **Patten IS, Rana S, Shahul S, Rowe GC, Jang C, Liu L, Hacker MR, Rhee JS, Mitchell J, Mahmood F, Hess P, Farrell C, Koulisis N, Khankin EV, Burke SD, Tudorache I, Bauersachs J, del Monte F, Hilfiker-Kleiner D, Karumanchi SA, and Arany Z**. Cardiac angiogenic imbalance leads to peripartum cardiomyopathy. *Nature* 485: 333-338, 2012.
36. **Planavila A, Dominguez E, Navarro M, Vinciguerra M, Iglesias R, Giralt M, Lope-Piedrafita S, Ruberte J, and Villarroya F**. Dilated cardiomyopathy and mitochondrial dysfunction in Sirt1-deficient mice: a role for Sirt1-Mef2 in adult heart. *J Mol Cell Cardiol* 53: 521-531, 2012.
37. **Puigserver P, Wu Z, Park CW, Graves R, Wright M, and Spiegelman BM**. A cold-inducible coactivator of nuclear receptors linked to adaptive thermogenesis. *Cell* 92: 829-839, 1998.
38. **Rasbach KA, Gupta RK, Ruas JL, Wu J, Naseri E, Estall JL, and Spiegelman BM**. PGC-1alpha regulates a HIF2alpha-dependent switch in skeletal muscle fiber types. *Proc Natl Acad Sci U S A* 107: 21866-21871, 2010.
39. **Riehle C, and Abel ED**. PGC-1 proteins and heart failure. *Trends Cardiovasc Med* 22: 98-105, 2012.
40. **Rowe GC, Jiang A, and Arany Z**. PGC-1 coactivators in cardiac development and disease. *Circ Res* 107: 825-838, 2010.
41. **Saffitz JE, Green KG, Kraft WJ, Schechtman KB, and Yamada KA**. Effects of diminished expression of connexin43 on gap junction number and size in ventricular myocardium. *Am J Physiol Heart Circ Physiol* 278: H1662-1670, 2000.
42. **Shepherd D, and Garland PB**. The kinetic properties of citrate synthase from rat liver mitochondria. *Biochem J* 114: 597-610, 1969.
43. **Trounce IA, Kim YL, Jun AS, and Wallace DC**. Assessment of mitochondrial oxidative phosphorylation in patient muscle biopsies, lymphoblasts, and transmitochondrial cell lines. *Methods Enzymol* 264: 484-509, 1996.
44. **Villena JA**. New insights into PGC-1 coactivators: redefining their role in the regulation of mitochondrial function and beyond. *The FEBS journal* 282: 647-672, 2015.
45. **Wang SC, Myers S, Dooms C, Capon R, and Muscat GE**. An ERRbeta/gamma agonist modulates GRalpha expression, and glucocorticoid responsive gene expression in skeletal muscle cells. *Mol Cell Endocrinol* 315: 146-152, 2010.
46. **Wang T, McDonald C, Petrenko NB, Leblanc M, Wang T, Giguere V, Evans RM, Patel VV, and Pei L**. Estrogen-related receptor alpha (ERRalpha) and ERRgamma are essential coordinators of cardiac metabolism and function. *Mol Cell Biol* 35: 1281-1298, 2015.
47. **Wende AR, Huss JM, Schaeffer PJ, Giguere V, and Kelly DP**. PGC-1alpha coactivates PDK4 gene expression via the orphan nuclear receptor ERRalpha: a mechanism for transcriptional control of muscle glucose metabolism. *Mol Cell Biol* 25: 10684-10694, 2005.
48. **Yu DD, and Forman BM**. Identification of an agonist ligand for estrogen-related receptors ERRbeta/gOrginalamma. *Bioorg Med Chem Lett* 15: 1311-1313, 2005.

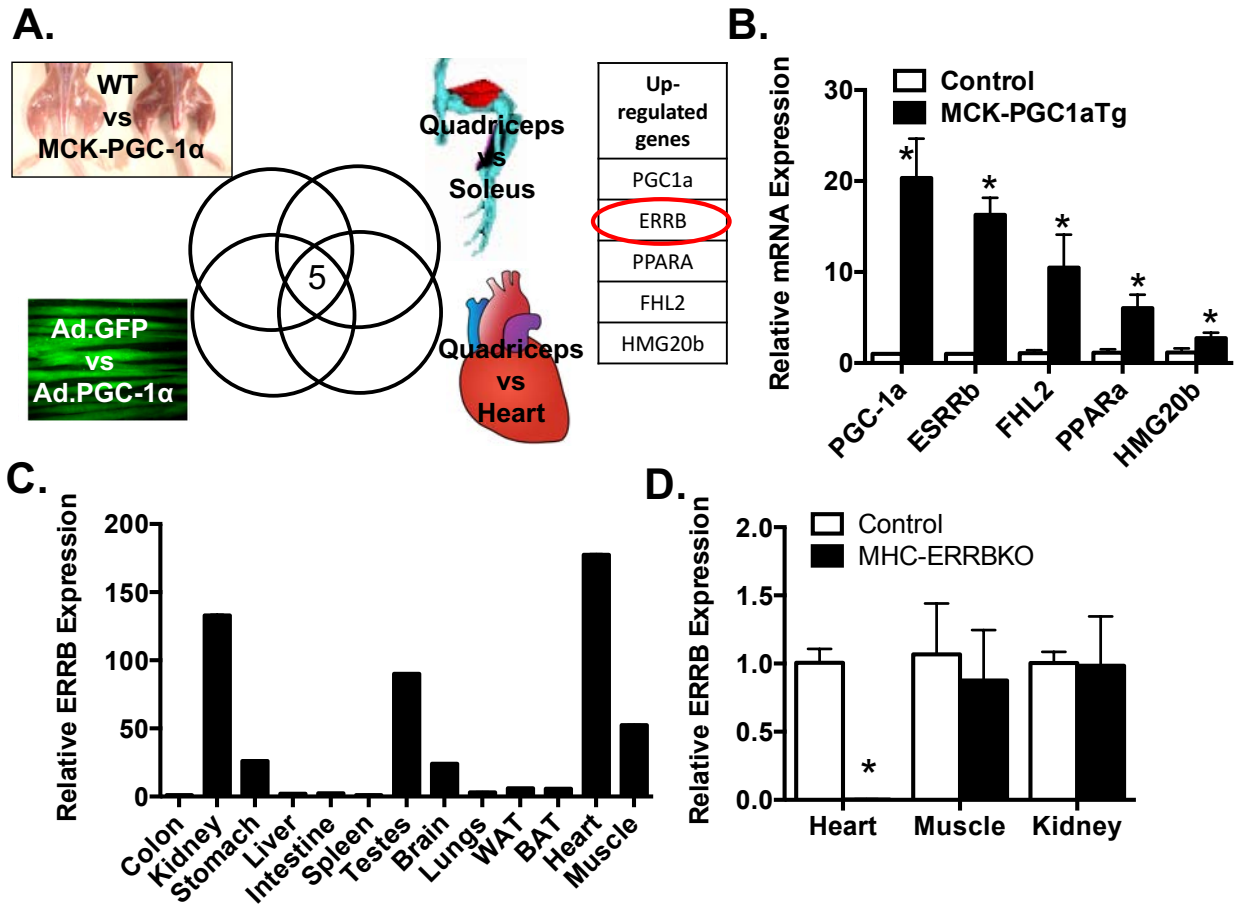
A.
WT
vs
MCK-PGC-1α
Ad.GFP
vs
Ad.PGC-1α
5
Quadriceps
vs
Soleus
Quadriceps
vs
Heart
Up-regulated genes
PGC1a
ERRB
PPARA
FHL2
HMG20b
B.
Relative mRNA Expression
Control
MCK-PGC1aTg
PGC-1a
ESRRb
FHL2
PPARa
HMG20b
C.
Relative ERRB Expression
Colon
Kidney
Stomach
Liver
Intestine
Spleen
Testes
Brain
Lungs
WAT
BAT
Heart
Muscle
D.
Relative ERRB Expression
Control
MHC-ERRBKO
Heart
Muscle
Kidney

Figure 1

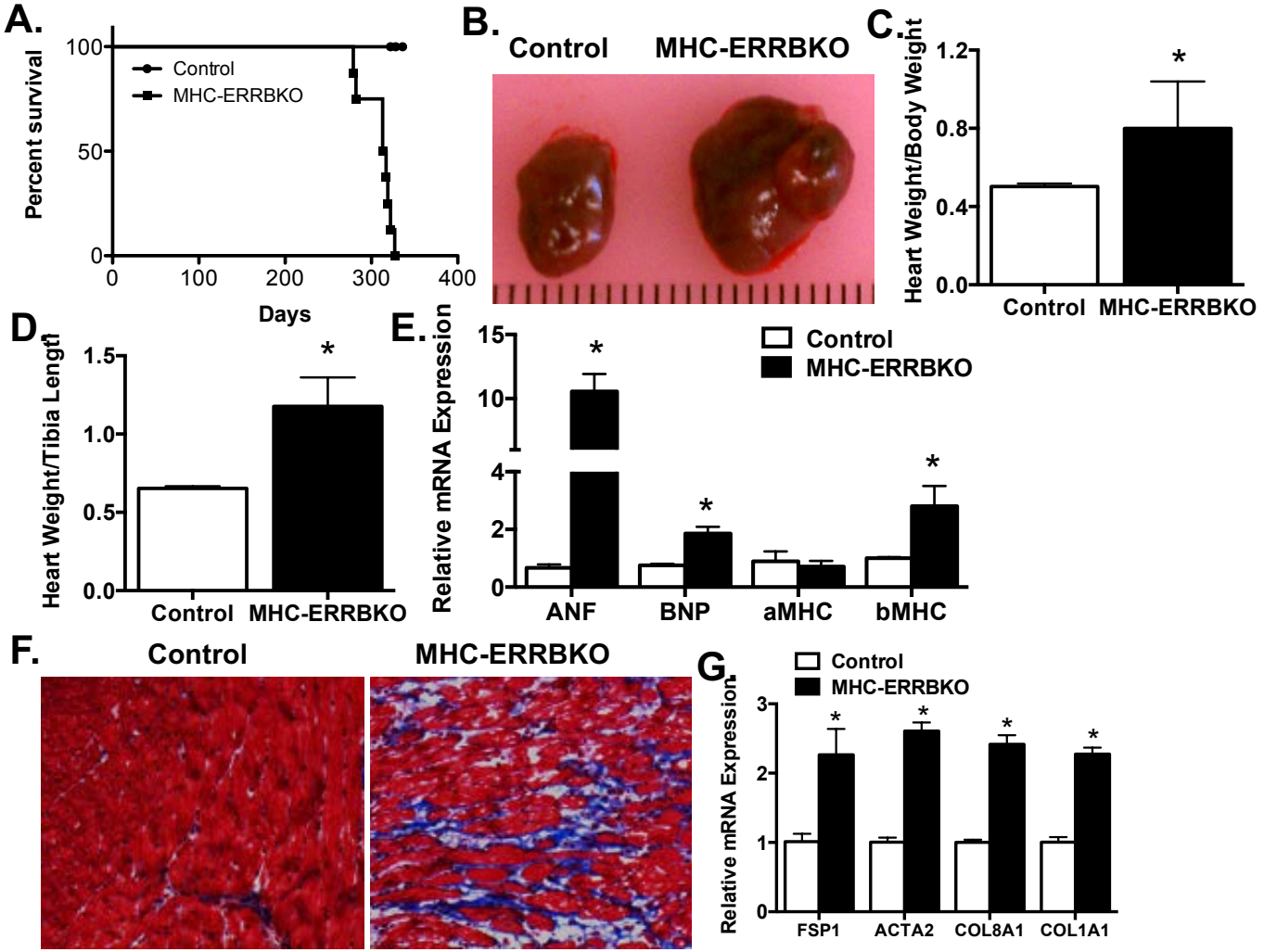
A.
Percent survival
100
50
0
Control
MHC-ERRBKO
0
100
200
300
400
Days
B.
Control
MHC-ERRBKO
C.
Heart Weight/Body Weight
1.2
0.8
0.4
0.0
*
Control
MHC-ERRBKO
D.
Heart Weight/Tibia Length
1.5
1.0
0.5
0.0
*
Control
MHC-ERRBKO
E.
Relative mRNA Expression
15
10
4
2
0
Control
MHC-ERRBKO
*
*
*
ANF
BNP
aMHC
bMHC
F.
Control
MHC-ERRBKO
G.
Relative mRNA Expression
Control
MHC-ERRBKO
3
2
1
0
*
*
*
*
FSP1
ACTA2
COL8A1
COL1A1

Figure 2

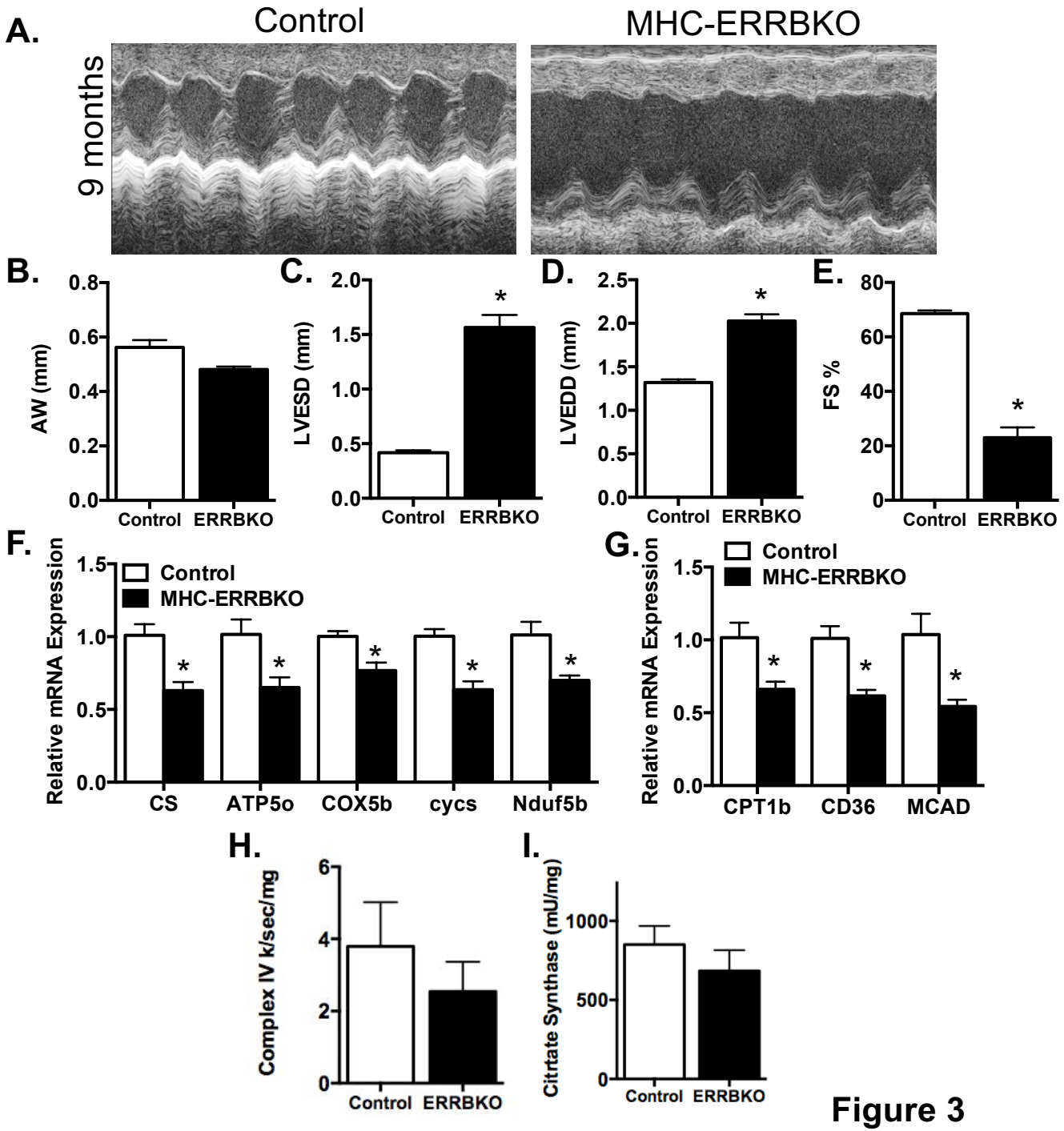
A.
Control
MHC-ERRBKO
9 months
B.
AW (mm)
0.0
0.2
0.4
0.6
0.8
Control
ERRBKO
C.
LVESD (mm)
0.0
0.5
1.0
1.5
2.0
*
Control
ERRBKO
D.
LVEDD (mm)
0.0
0.5
1.0
1.5
2.0
2.5
*
Control
ERRBKO
E.
FS %
0
20
40
60
80
*
Control
ERRBKO
F.
Relative mRNA Expression
Control
MHC-ERRBKO
0.0
0.5
1.0
1.5
*
CS
ATP5o
COX5b
cycs
Nduf5b
G.
Relative mRNA Expression
Control
MHC-ERRBKO
0.0
0.5
1.0
1.5
*
CPT1b
CD36
MCAD
H.
Complex IV k/sec/mg
0
2
4
6
Control
ERRBKO
I.
Citrtate Synthase (mU/mg)
0
500
1000
Control
ERRBKO

Figure 3

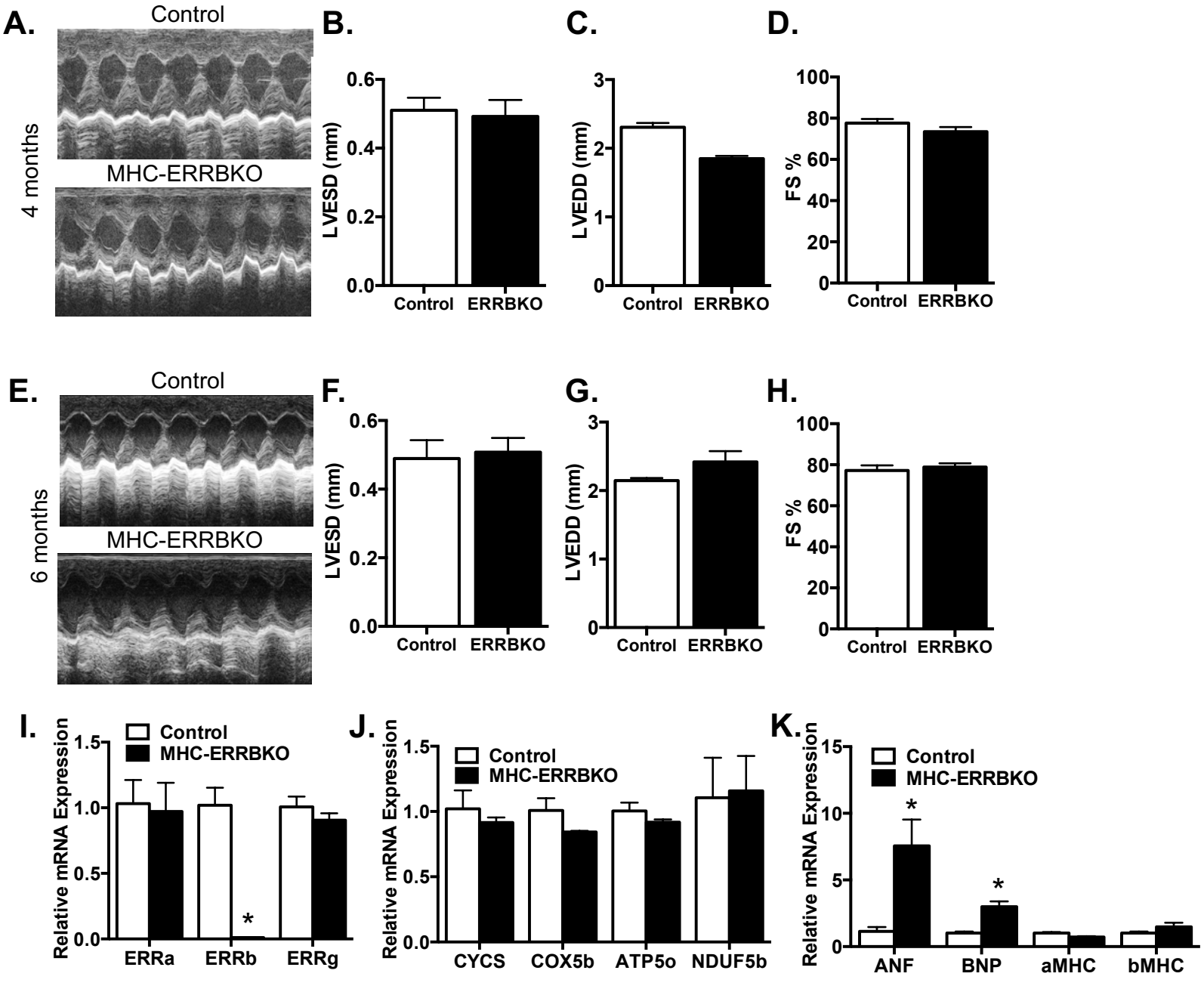
A.
Control
4 months
MHC-ERRBKO
B.
LVESD (mm)
0.6
0.4
0.2
0.0
Control
ERRBKO
C.
LVEDD (mm)
3
2
1
0
Control
ERRBKO
D.
FS %
100
80
60
40
20
0
Control
ERRBKO
E.
Control
6 months
MHC-ERRBKO
F.
LVESD (mm)
0.6
0.4
0.2
0.0
Control
ERRBKO
G.
LVEDD (mm)
3
2
1
0
Control
ERRBKO
H.
FS %
100
80
60
40
20
0
Control
ERRBKO
I.
Relative mRNA Expression
Control
MHC-ERRBKO
1.5
1.0
0.5
0.0
*
ERRa
ERRb
ERRg
J.
Relative mRNA Expression
Control
MHC-ERRBKO
1.5
1.0
0.5
0.0
CYCS
COX5b
ATP5o
NDUF5b
K.
Relative mRNA Expression
Control
MHC-ERRBKO
15
10
5
0
*
*
ANF
BNP
aMHC
bMHC

Figure 4

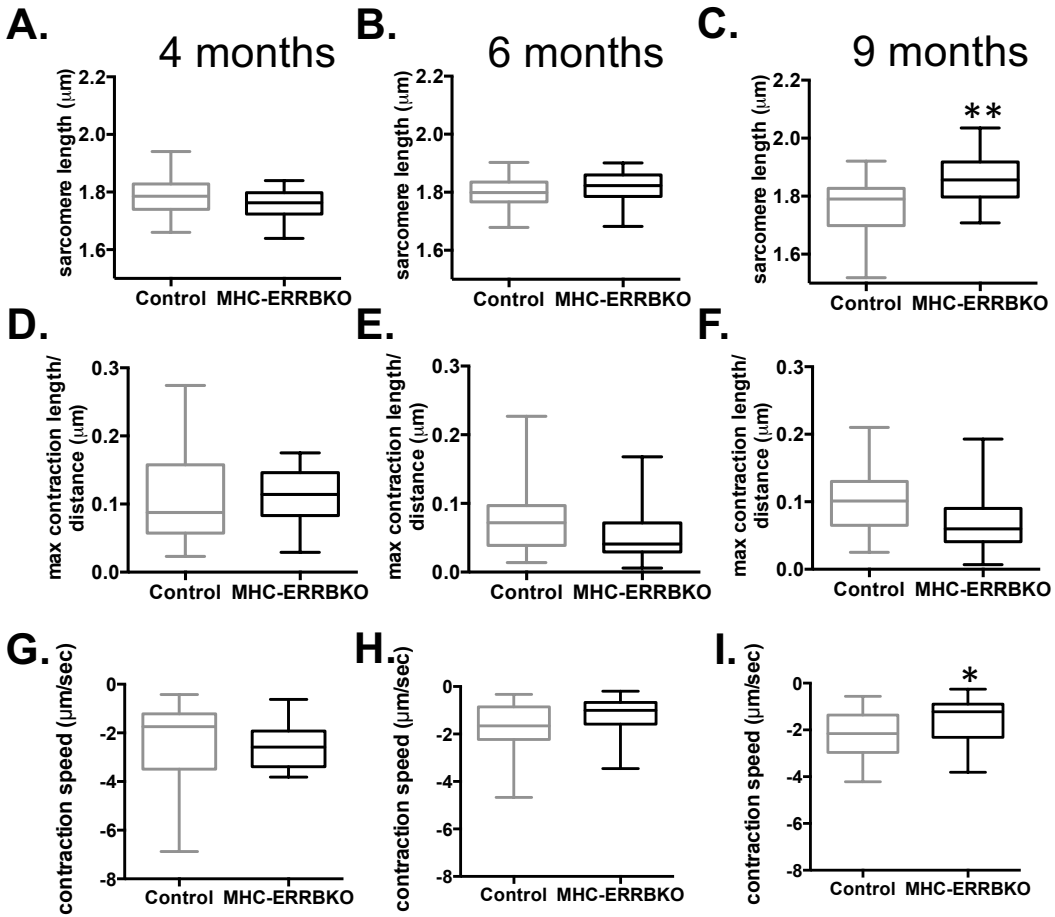
A.
4 months
B.
6 months
C.
9 months
sarcomere length (μm)
2.2
2.0
1.8
1.6
**
Control
MHC-ERRBKO
D.
E.
F.
max contraction length/ distance (μm)
0.3
0.2
0.1
0.0
G.
H.
I.
contraction speed (μm/sec)
0
-2
-4
-6
-8
*

Figure 5

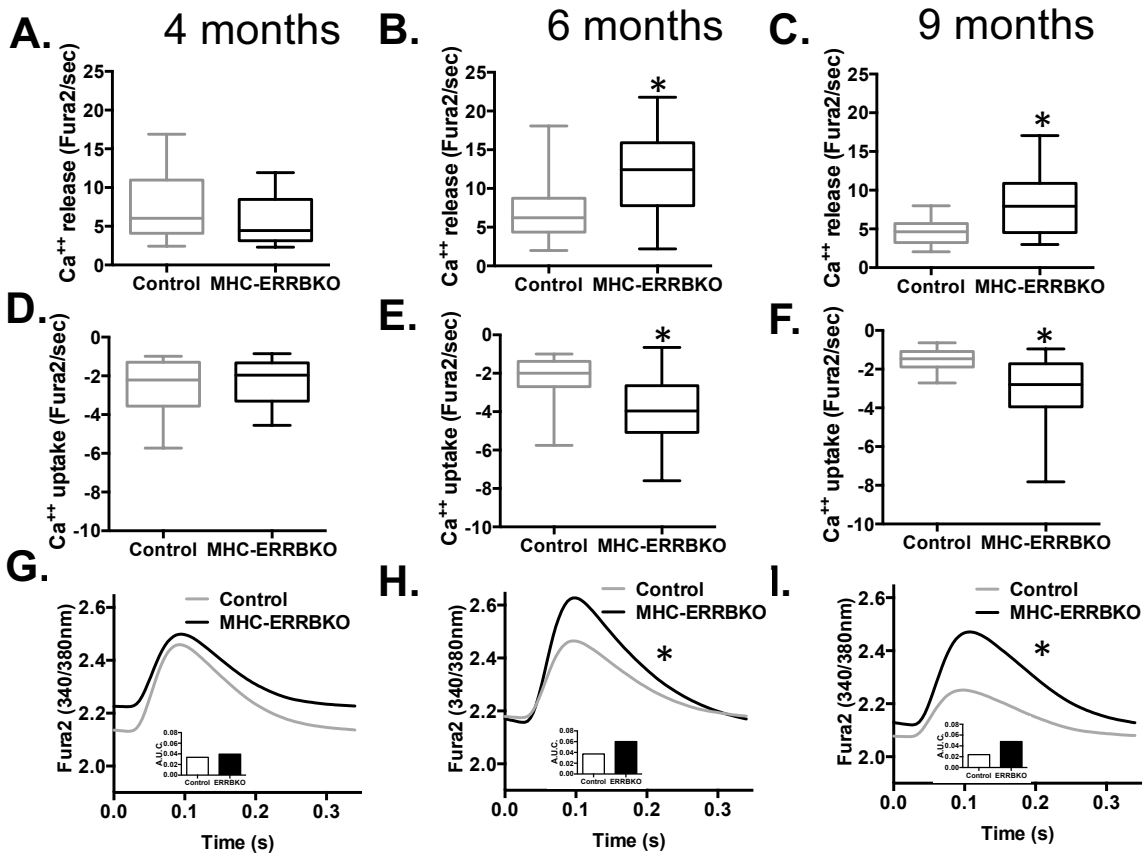
A.
4 months
B.
6 months
C.
9 months
Ca++ release (Fura2/sec)
Control
MHC-ERRBKO
D.
E.
F.
Ca++ uptake (Fura2/sec)
G.
H.
I.
Fura2 (340/380nm)
Time (s)
A.U.C.
ERRBKO

Figure 6

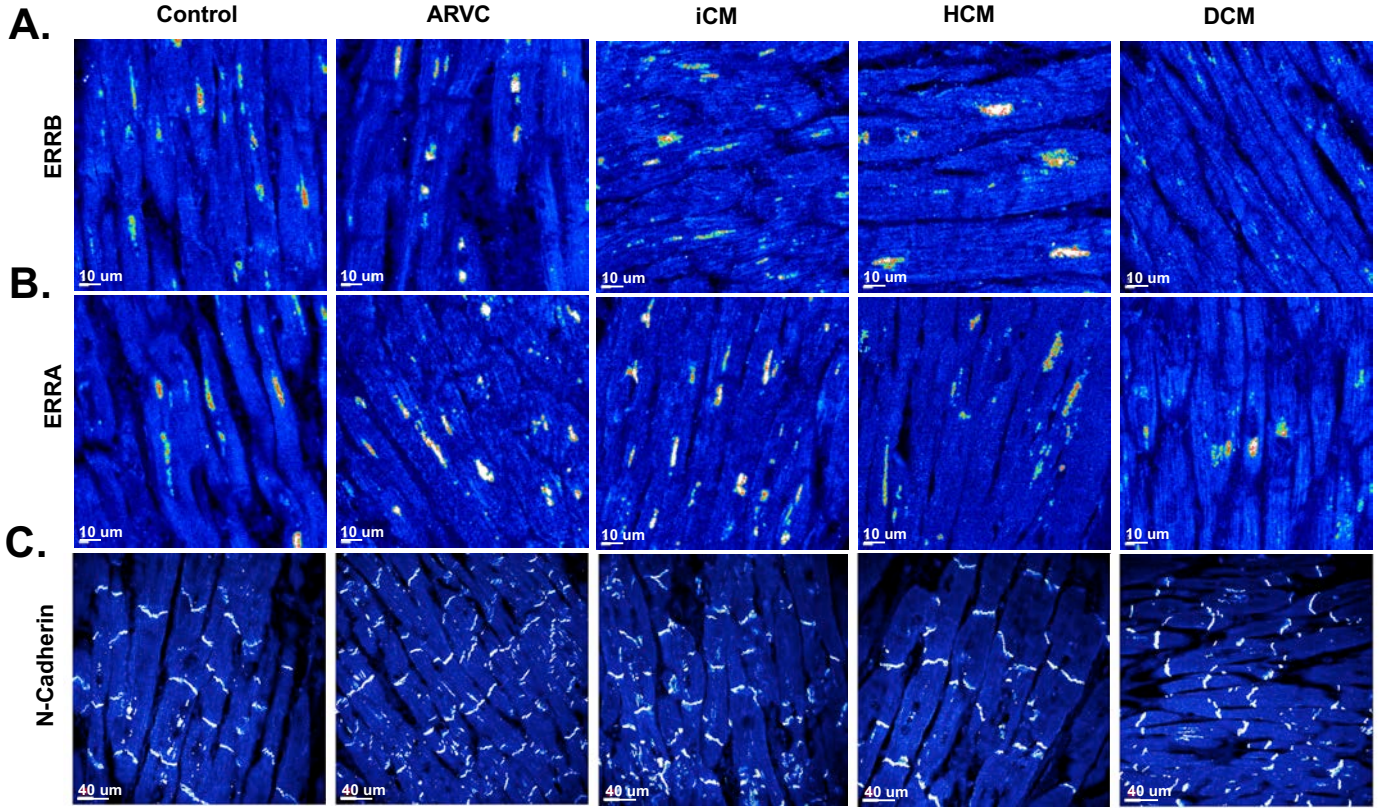
A.
Control
ARVC
iCM
HCM
DCM
ERRB
B.
ERRA
C.
N-Cadherin
10 um
40 um

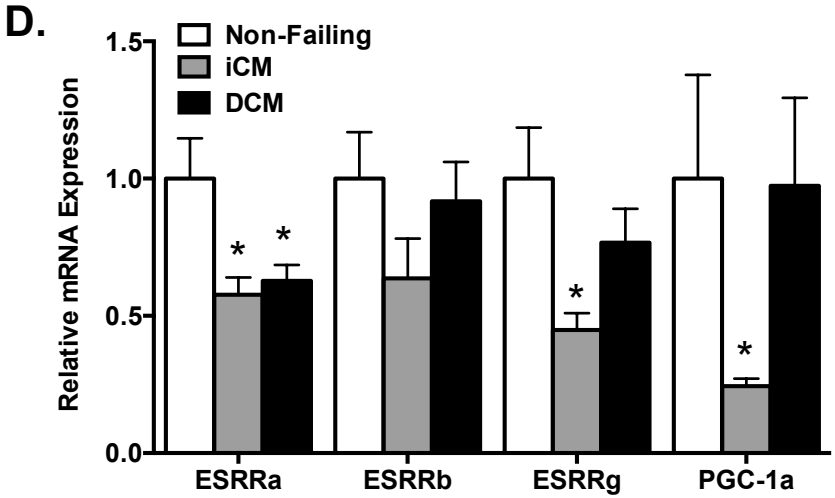
D.
Non-Failing
iCM
DCM
Relative mRNA Expression
1.5
1.0
0.5
0.0
*
ESRRa
ESRRb
ESRRg
PGC-1a

Figure 7